

Article

Palladium-Rhenium Catalysts for Selective Hydrogenation of Furfural: Influence of Catalyst Preparation on Structure and Performance

Simon T. Thompson and H. Henry Lamb *

Department of Chemical and Biomolecular Engineering, North Carolina State University, Raleigh, NC 27695-7905, USA; simon.thompson@ee.doe.gov

* Correspondence: lamb@ncsu.edu; Tel.: +1-919-515-6395

Abstract: PdRe/Al₂O₃ catalysts are highly selective for hydrogenation of furfural to furfuryl alcohol (FAL). Moreover, the synergy between the metals can result in greater specific activity (higher turnover frequency, TOF) than exhibited by either metal alone. Bimetallic catalyst structure depends strongly on the metal precursors employed and their addition sequence to the support. In this work, PdRe/Al₂O₃ catalysts were prepared by: (i) co-impregnation (CI) and sequential impregnation (SI) of γ -Al₂O₃ using HReO₄ and Pd(NO₃)₂, (ii) SI using NH₄ReO₄ and [Pd(NH₃)₄(NO₃)₂], (iii) HReO₄ addition to a reduced and passivated Pd/Al₂O₃ catalyst, and (iv) impregnation with the double complex salt (DCS), [Pd(NH₃)₄(ReO₄)₂]. Raman spectroscopy and temperature-programmed reduction (TPR) evidence larger supported PdO crystallites in catalysts prepared using Pd(NO₃)₂ than [Pd(NH₃)₄(NO₃)₂]. Surface [ReO₄]⁻ species detected by Raman exhibit TPR peak temperatures from ranging 85 to 260 °C (versus 375 °C for Re/Al₂O₃). After H₂ reduction at 400 °C, the catalysts were characterized by chemisorption, temperature-programmed hydride decomposition (TPHD), CO diffuse reflectance infrared Fourier transform spectroscopy (DRIFTS), and scanning transmission electron microscopy (STEM) with energy-dispersive x-ray (EDX) spectroscopy. The CI catalyst containing supported Pd–Re alloy crystallites had a TOF similar to Pd/Al₂O₃ but higher (61%) FAL selectivity. In contrast, catalysts prepared by methods (ii–iv) containing supported Pd–Re nanoparticles exhibit higher TOFs and up to 78% FAL selectivity.



Citation: Thompson, S.T.; Lamb, H.H. Palladium-Rhenium Catalysts for Selective Hydrogenation of Furfural: Influence of Catalyst Preparation on Structure and Performance. *Catalysts* **2023**, *13*, 1239. <https://doi.org/10.3390/catal13091239>

Academic Editors: Shihui Zou and Juanjuan Liu

Received: 16 July 2023

Revised: 15 August 2023

Accepted: 23 August 2023

Published: 25 August 2023



Copyright: © 2023 by the authors. Licensee MDPI, Basel, Switzerland. This article is an open access article distributed under the terms and conditions of the Creative Commons Attribution (CC BY) license (<https://creativecommons.org/licenses/by/4.0/>).

Keywords: bimetallic catalysts; Raman spectroscopy; TPR; palladium hydride; chemisorption; DRIFTS; STEM-EDX

1. Introduction

Rhenium is used in supported bimetallic catalysts with other Group VIII metals (such as Rh [1–4], Ru [5,6], and Pd [7]) to enhance selective hydrogenation and hydrogenolysis of oxygenated organic compounds. Tomishige and coworkers investigated SiO₂- and C-supported Re bimetallic catalysts for a variety of reactions, including ester hydrogenolysis [2], ring-opening of cyclic ethers [1,4], hydrogenation of fatty acids to alcohols [7], and glycerol hydrogenolysis [8]. For each reaction, Re addition boosts activity and selectivity to the desired product, e.g., 1,5-pentanediol from the ring-opening of tetrahydrofurfuryl alcohol [4]. Similarly, Re addition to Pd/SiO₂ increased selectivity to fatty alcohols in fatty acid hydrogenation [7]. The suppression of CO chemisorption (compared to Rh/SiO₂) and the observed modification of catalytic activity suggested surface modification of supported Rh particles by Re species. Complementary results from extended x-ray absorption fine structure (EXAFS) spectroscopy, x-ray photoelectron spectroscopy (XPS), x-ray diffraction, and scanning transmission electron microscopy with energy-dispersive x-ray analysis (STEM-EDX) led to the conclusion that low-valent ReO_x species in contact with supported Rh particles were the active sites [4,9]. Supported PdRe catalysts also have been investi-

gated for selective hydrogenation of dicarboxylic acids [10–12], hydrodechlorination [13,14], and reforming reactions [15].

Structural investigations of PdRe/Al₂O₃ catalysts have been limited. Meitzner et al. examined a 0.6 wt.% Pd–1 wt.% Re/Al₂O₃ catalyst prepared by incipient wetness (IW) co-impregnation (CI) by EXAFS spectroscopy and inferred Pd–Re alloy formation [16]. Ziemecki et al. investigated PdRe/Al₂O₃ catalysts prepared by sequential impregnation (SI): depositing a Pd²⁺ salt on γ -Al₂O₃, calcining, reducing to Pd⁰, passivating, and then adding the Re precursor [17,18]. Characterization of the resultant catalyst by temperature-programmed reduction (TPR), H₂ uptake measurements, and in situ x-ray diffraction (XRD) demonstrated that substitutional alloying with Re was responsible for the suppression of bulk palladium hydride (PdH_x) formation. Karpinski and coworkers used a similar preparation method and also reported PdH_x suppression associated with Pd–Re alloy formation based on XRD and temperature-programmed hydride decomposition (TPHD) [13–15]. Because the addition of small amounts of Re to Pd/Al₂O₃ suppressed CO chemisorption and inhibited hydroisomerization activity, they concluded that Re occupied the surface of Pd-rich alloy particles [14]. More recently, Holles and coworkers used directed deposition to selectively form Pd overlayers on alumina-supported Re particles [19,20]; the catalysts were characterized primarily by H₂ chemisorption and a simple probe reaction (ethylene hydrogenation).

Our previous research on PdRe/Al₂O₃ catalysts for selective hydrogenation of furfural to furfuryl alcohol (FAL) demonstrated substantial differences in catalyst structure and performance depending on the preparation method, metal precursors, and Pd:Re ratio [21]. A strong correlation between selective hydrogenation activity and suppression of H₂ chemisorption was observed. The H/CO chemisorption ratio at 35 °C correlated with furfuryl turnover frequency (TOF) and FAL selectivity, and there was an optimum surface composition. PdRe/Al₂O₃ catalysts with 1:2 Pd:Re molar ratios (exhibiting very low H/CO ratios) had low activity suggesting that the Pd surface was covered by Re. More recently, Kammert et al. investigated PdRe/SiO₂ and PdRe/TiO₂ catalysts for the hydrogenation of propionic acid and proposed that Pd facilitates the reaction by dissociating H₂ providing hydrides and protons to vicinal Re sites [22].

In this work, we further elucidate the structures of PdRe/Al₂O₃ catalysts for selective hydrogenation of furfural using TPR, TPHD, CO and H₂ chemisorption, CO diffuse reflectance infrared Fourier transform spectroscopy (DRIFTS), and STEM-EDX. The roles of the metal precursors, impregnation sequence, and calcination conditions in determining catalyst morphology (i.e., particle size and metal-metal interactions) are investigated. Moreover, we take advantage of the strong Raman bands of the perrhenate ion, [ReO₄][−], and PdO crystallites to characterize the as-prepared catalysts. Otto et al. measured the Raman spectra of a series of Pd/Al₂O₃ catalysts and found a linear relationship between the intensity of the PdO B_{1g} lattice vibration and Pd loading (up to 2.5 wt.%) [23]. Baylet et al. used in situ Raman spectroscopy to investigate the dynamics of Pd/Al₂O₃ oxidation catalysts [24]. Re/Al₂O₃ catalysts have been probed extensively by Raman spectroscopy [25–27], but we are not aware of any studies of PdRe/Al₂O₃ catalysts. To facilitate Raman spectroscopy, a new series of PdRe/Al₂O₃ catalysts was prepared using a γ -Al₂O₃ support that did not fluoresce strongly in the region of interest. Specifically, catalysts were prepared by: (i) CI and SI of γ -Al₂O₃ using HReO₄ and Pd(NO₃)₂, (ii) SI using NH₄ReO₄ and [Pd(NH₃)₄(NO₃)₂] (intermediate and final calcination steps), (iii) SI via HReO₄ addition to a reduced and passivated Pd/Al₂O₃ catalyst, and (iv) impregnation with the double complex salt (DCS), [Pd(NH₃)₄(ReO₄)₂].

2. Results and Discussion

2.1. Catalyst Characterization

The catalysts, metal precursors, and loadings are listed in Table 1. The catalyst name denotes the metal(s), target loading(s) (wt.%), and metal precursor(s): nitrate, N or tetraamine nitrate, TA for Pd, and perrhenic acid, H or ammonium perrhenate, N for Re. Co-

impregnation and sequential impregnation are indicated by CI and SI, respectively. The impregnation sequence (for SI) is indicated by the order of metals (e.g., Re-first 5 wt.%, Pd 3 wt.% = Re5Pd3). Values in parentheses indicate different calcination temperatures for this catalyst formulation. DCS indicates impregnation with the stoichiometric double complex salt, $[\text{Pd}(\text{NH}_3)_4(\text{ReO}_4)_2]$.

Table 1. Precursors and compositions of $\gamma\text{-Al}_2\text{O}_3$ -supported catalysts.

Catalyst	Metal Precursor(s)	Pd Loading ^a (wt.%)	Re Loading ^a (wt.%)
Pd1-N	$\text{Pd}(\text{NO}_3)_2$	0.91	-
Pd3-N	$\text{Pd}(\text{NO}_3)_2$	2.66	-
Pd3-TA	$\text{Pd}(\text{NH}_3)_4(\text{NO}_3)_2$	2.34	-
Pd3Re5-CI	$\text{Pd}(\text{NO}_3)_2$ and HReO_4	2.43	4.41
Pd3Re5-SI	$\text{Pd}(\text{NH}_3)_4(\text{NO}_3)_2$ and HReO_4	2.80	4.63
Re5Pd3N-SI	HReO_4 and $\text{Pd}(\text{NO}_3)_2$	2.15	5.73
Re5Pd3-SI (350)	NH_4ReO_4 and $\text{Pd}(\text{NH}_3)_4(\text{NO}_3)_2$	2.56	4.23
Re5Pd3-SI (400)	NH_4ReO_4 and $\text{Pd}(\text{NH}_3)_4(\text{NO}_3)_2$	2.27	4.24
Re5Pd1.5-DCS	$\text{Pd}(\text{NH}_3)_4(\text{ReO}_4)_2$	1.42	4.65
Re5-H	HReO_4	-	5.29
Re5-N	NH_4ReO_4	-	4.54

^a Inductively coupled plasma-optical emission spectrometry (ICP-OES) measurements.

Raman spectra of the as-prepared 3 wt.% Pd/ Al_2O_3 catalysts (Figure 1a) contain a peak at $\sim 640\text{ cm}^{-1}$ corresponding to the B_{1g} lattice vibration of PdO crystallites [28]. This peak has negligible intensity in the Raman spectrum of the as-prepared Pd1-N catalyst (not shown). It has been observed at 626 to 651 cm^{-1} in supported Pd catalysts and PdO thin films [23,24,29–31]. A weak Raman peak at $\sim 280\text{ cm}^{-1}$ is also observed, which was attributed by McBride et al. to a second-order scattering process [28]. Another Raman band at 445 cm^{-1} was assigned to the E_g lattice vibration; however, McBride et al. note that the band is extremely weak when employing 632.8 nm (He–Ne laser) excitation [28]. Otto et al. [23] found that the integrated intensity of the B_{1g} lattice vibration was directly proportional to Pd loading (0.2–2.5 wt.% range) in fully oxidized Pd/ Al_2O_3 catalysts. They suggested that highly dispersed PdO crystallites smaller than $\sim 1.5\text{ nm}$ (containing fewer than ca. 50 metal atoms) interacting with the $\gamma\text{-Al}_2\text{O}_3$ support were undetectable by Raman spectroscopy.

Despite their similar Pd loadings, the Raman B_{1g} band of Pd3-N is much stronger and shifted slightly to lower wavenumbers than that of Pd3-TA leading us to infer that the Pd3-N catalyst contains larger PdO crystallites. The smaller PdO particle size (i.e., higher dispersion) achieved using the tetraammine nitrate precursor can be explained by strong electrostatic adsorption (SEA) [32]. The pH of the $[\text{Pd}(\text{NH}_3)_4(\text{NO}_3)_2]$ impregnation solution was well above the point-of-zero charge (PZC) of $\gamma\text{-Al}_2\text{O}_3$ (8.0 ± 0.2) resulting in a net negative charge on the support. Specifically, surface hydroxyl groups are deprotonated leaving surface O^- ions that electrostatically attract $[\text{Pd}(\text{NH}_3)_4]^{2+}$ cations. In contrast, $\text{Pd}(\text{NO}_3)_2$ solutions are neutral to slightly acidic (pH below PZC of $\gamma\text{-Al}_2\text{O}_3$), and the SEA effect is negated.

Raman spectra of the as-prepared Re/ Al_2O_3 catalysts (Figure 1a) contain peaks corresponding to rhenium-oxygen stretching and bending modes. The strong sharp peak at 970 cm^{-1} is assigned to the symmetric Re=O stretching mode (ν_s) of T_d $[\text{ReO}_4]^-$ species [25–27]. The peak position corresponds to perrhenate ion in aqueous solution, as expected following exposure to ambient moisture. Additional bands at 920 (vw) and $335\text{ (w)}\text{ cm}^{-1}$ are assigned to the antisymmetric Re=O stretching (ν_{as}) and O–Re–O bending (δ) modes, respectively. Significantly, no Raman bands indicative of Re–O–Re bonding are observed consistent with submonolayer coverage of isolated perrhenate species on $\gamma\text{-Al}_2\text{O}_3$. A small peak appears at 1000 cm^{-1} in the Raman spectrum of Re5-H. The symmetric Re=O stretching peak is shifted to $\sim 1000\text{ cm}^{-1}$ for a hypothetical C_{3v} $[\text{ReO}_4]$ species with three

identical Re=O bonds and a Re–O–Al bridge to the support [25,33]; however, this species typically is found only under dehydrated conditions [26,27].

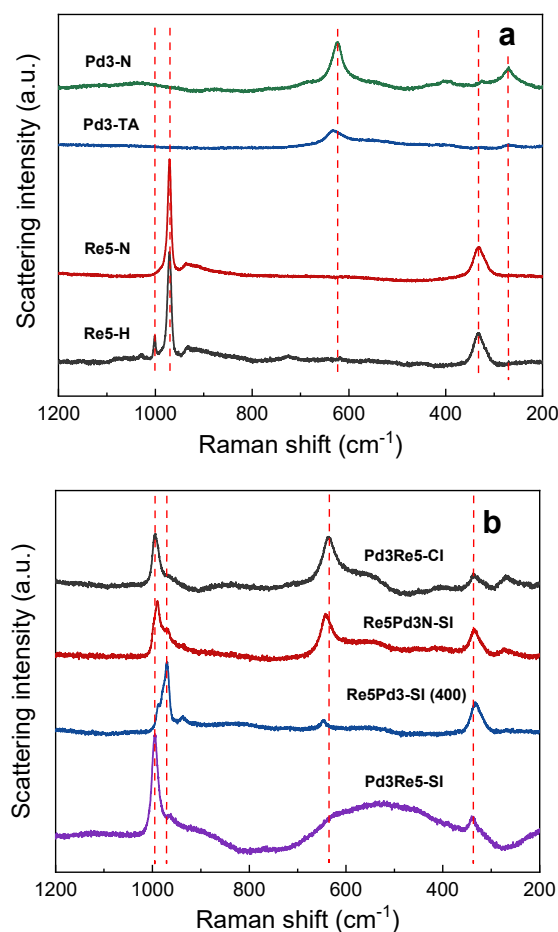


Figure 1. Raman spectra of Pd/Al₂O₃ and Re/Al₂O₃ catalysts (a) and PdRe/Al₂O₃ catalysts (b).

The strong PdO band (B_{1g} mode) in the Raman spectrum of Pd3Re5-Cl evidences that PdO crystallites are present following calcination (Figure 1b). A strong shoulder at ~ 550 cm⁻¹ and a weak band at ~ 280 cm⁻¹ are also observed. A medium-intensity $\nu_s(\text{Re}=\text{O})$ band at ~ 1000 cm⁻¹ and weak $\delta(\text{O}-\text{Re}-\text{O})$ band at 335 -cm⁻¹ are observed consistent with isolated $[\text{ReO}_4]^-$ species. An unassigned weak broad feature at ~ 850 cm⁻¹ is also noted. The Raman spectrum of Re5Pd3N-SI, another bimetallic catalyst prepared from Pd(NO₃)₂, is closely similar. Qualitatively, the $\nu_s(\text{Re}=\text{O})$ bands for these bimetallic catalysts are broader and less intense than those for Re5-H and Re5-N (Figure 1a). The strong intensity of the B_{1g} mode is indicative of supported PdO crystallites. The medium-intensity $\nu_s(\text{Re}=\text{O})$ band contains at least two components between 1000 and 970 cm⁻¹ indicating $[\text{ReO}_4]^-$ species in different environments.

In contrast, the PdO B_{1g} mode in the Raman spectrum of Re5Pd3-SI (400) (Figure 1b) is very weak and shifted to slightly higher wavenumbers indicating that only small PdO nanoparticles and/or isolated Pd oxo complexes are present after the final calcination. These results suggest that the size and distribution of PdO particles after calcination are affected more strongly by the metal precursor than by the method of preparation. We infer that SEA of the tetraammine complex to the ReO_x-modified support results in highly dispersed Pd oxo species. A strong $\nu_s(\text{Re}=\text{O})$ peak is observed at 970 cm⁻¹ with a shoulder at ~ 1000 cm⁻¹. The $\nu_{as}(\text{Re}=\text{O})$ and $\delta(\text{O}-\text{Re}-\text{O})$ peaks at 920 and 335 cm⁻¹, respectively, allow a definitive assignment to T_d $[\text{ReO}_4]^-$. The PdO B_{1g} band has a negligible intensity in the Raman spectrum of Pd3Re5-SI (Figure 1b). Instead, a large, broad feature at 300 – 700 cm⁻¹ due to fluorescence from the γ -Al₂O₃ support is observed. Otto et al. inferred that fluorescence in

this region is quenched by a PdO-support interaction [23]. Consistent with this hypothesis, fluorescence is suppressed for the other catalysts examined herein. In Pd3Re5-SI, Pd was reduced and passivated prior to impregnation with HReO₄. The absence of a low-temperature TPR peak (*vide infra*) indicates that the Pd⁰ particles are not converted to bulk PdO, and we infer that a thin PdO_x layer is formed consistent with the oxidation mechanism proposed by Su et al. [29]. The strong Raman band at 1000 cm⁻¹ is assigned to [ReO₄]⁻ species interacting with support and/or the PdO_x-covered metal particles.

TPR profiles of the as-prepared 3% Pd/AlO₃ catalysts are shown in Figure 2a. Reduction of larger supported PdO crystallites in Pd3-N (observed by Raman) occurs abruptly at sub-ambient temperatures resulting in a very sharp H₂ uptake peak at approximately -10 °C. An additional H₂ uptake feature at ~30 °C is ascribed to reversible PdH_x formation; H₂ evolution associated with PdH_x decomposition is observed at ~55 °C. TPR profiles of two Pd3-TA catalysts (A and B) prepared using different alumina supports are also shown. The TPR profile for Pd3-TA (A) (prepared using the same support as the other catalysts in this work) is broader and reduction occurs at higher temperatures consistent with PdO nanoparticles interacting strongly with the γ-Al₂O₃ support and/or surface-bound Pd oxo complexes. There is a shallow dip in the TCD signal at ~55 °C consistent with PdH_x decomposition followed by a broad maximum at ~80 °C. The small H₂ consumption feature at 290 °C arises from the reduction of carbonate species associated with alkali and alkaline impurities, as confirmed by CH₄ evolution [34]. In contrast, H₂ consumption during TPR of Pd3-TA (B) occurs primarily at <50 °C. Because Pd⁰ particles are formed at low temperatures, H₂ is evolved at 55 °C (inverse peak) due to β-PdH_x decomposition. H₂ uptake continues to ~200 °C. Because γ-Al₂O₃ (B) lacks the alkali and alkaline metal impurities of γ-Al₂O₃ (A), a H₂ uptake feature at 290 °C is not observed. Quantitative H₂ uptake measurements [excluding the 290 °C peak for Pd3-TA (A)] (Table 2) indicate a complete reduction of Pd²⁺ to Pd⁰ following TPR to 400 °C. The TPR profile of Re5-N (Figure 2b) contains a well-defined peak at 375 °C with a high-temperature tail extending to ~700 °C. TPR peak position and shape for Re5-H are similar (not shown). Quantitative H₂ uptake measurements (Table 2) indicate incomplete reduction of Re⁷⁺ after TPR to 400 °C; however, complete reduction to Re⁰ was achieved after TPR to 800 °C.

The TPR profiles of bimetallic catalysts prepared using HReO₄ and Pd(NO₃)₂ are qualitatively similar (Figure 2b). An extremely sharp peak attributed to the reduction of PdO crystallites is observed at ~25 °C. Although similar to the low-temperature TPR peak observed for Pd3-N, it occurs at ~20 °C higher temperature. A second low-temperature TPR peak appears at ~55–60 °C that may be assigned to Pd or Re species. The higher temperature (>100 °C) TPR features are consistent with Re reduction. The maximum rate of H₂ consumption occurs at ~260 °C—more than 100 °C below the peak reduction temperature of Re5-N. Facilitated reduction of perrhenate species in PdRe/Al₂O₃ catalysts has been ascribed to (i) hydrogen spillover from Pd particles [21] and (ii) migration of Re₂O₇ to Pd particles in the presence of adsorbed H₂O [18]. In contrast to Re5-N, the TPR of Pd3Re5-CI evidences that essentially all supported Re has been reduced after heating to 400 °C in 5% H₂/Ar (Table 2).

Table 2. TPR and TPHD results for selected catalysts.

Catalyst	H/Metal Ratio (TPR) ¹	Re Oxidation State (TPR) ²	H/Pd (TPHD) ⁴
Pd3-N	2.1	-	0.32
Pd3-TA	2.4	-	0.13
Pd3Re5-CI	4.4	0.4	0.063
Pd3Re5-SI	3.6	0.7 ³	0.058
Re5Pd3N-SI	5.0	0.7	0.18
Re5Pd3-SI (350)	4.3	0.3	0.11
Re5Pd3-SI (400)	4.5	0.2	0.12
Re5-N	4.9	2.1	--

¹ Based on TPR H₂ consumption to 400 °C. ² For PdRe catalysts, assume 2.0 H/Pd with the balance to Re⁷⁺ reduction. ³ Based on TPR H₂ consumption by Pd3-TA after reduction and passivation. ⁴ Based on H₂ evolution at >0 °C.

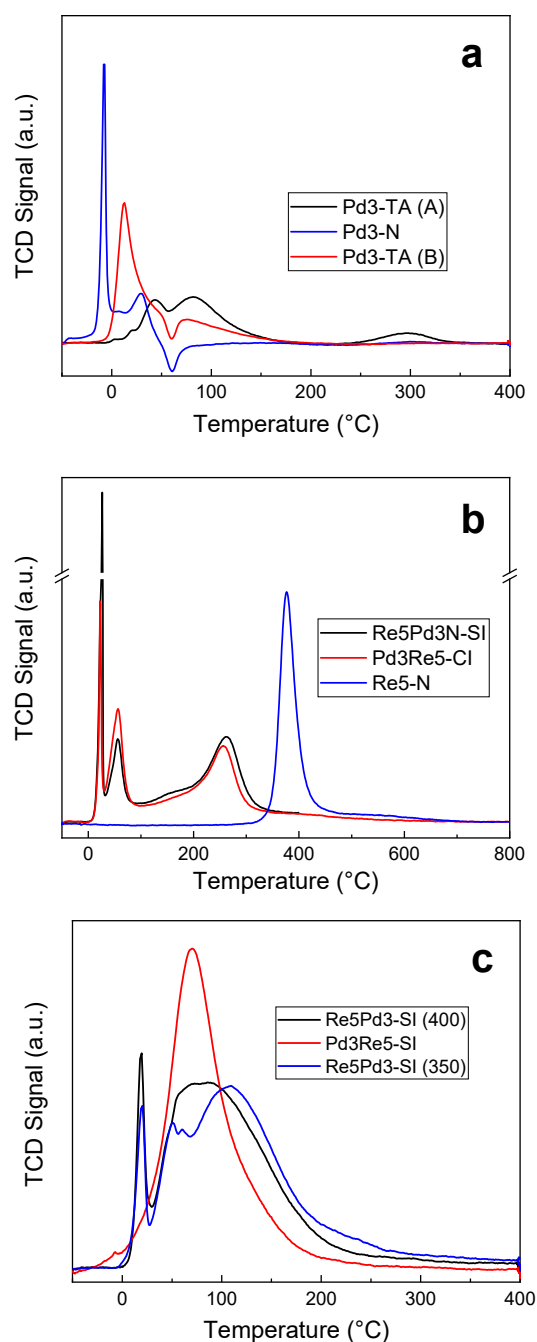


Figure 2. TPR profiles of Pd/Al₂O₃ (a), Re/Al₂O₃ (b), and PdRe/Al₂O₃ catalysts (b,c). Preparation and characterization of Pd3-N (B) described in [21].

The bimetallic catalysts Re5Pd3-SI (350) and Re5Pd3-SI (400) have similar TPR profiles (Figure 2c) comprising a sharp Pd reduction peak at ~10 °C and a broad Re reduction feature at 30–200 °C. The Pd reduction peak is sharper and occurs at lower temperatures than for Pd3-TA (A) suggesting that the presence of supported perrhenate species affects Pd²⁺ reduction. Most Re reduction occurs at <200 °C consistent with hydrogen spillover from highly dispersed Pd particles [21]. Essentially, complete Re reduction is obtained for both catalysts at 400 °C (Table 2). Increasing the calcination temperature and time to 3 h sharpens the peaks and lowers the Re reduction temperature. The converse would be expected for moisture-dependent diffusion of ReO_x species to Pd⁰ particles. The TPR profile of Pd3Re5-SI exhibits a single symmetric peak with a maximum of ~80 °C. Ziemecki et al. reported a similar TPR profile (47 °C peak maximum) for a PdRe/Al₂O₃

catalyst prepared by impregnation of a reduced 3 wt.% Pd/Al₂O₃ catalyst with aqueous Re₂O₇ and dehydration at 110 °C [18]. Malinowski et al. [13] also reported a complete reduction of similarly prepared PdRe/Al₂O₃ catalysts after heating H₂ at 400 °C for 3 h. Ziemecki et al. inferred that Re₂O₇ mobility on the hydroxylated γ -Al₂O₃ surface was the underlying mechanism of low-temperature Re reduction because dehydroxylation at 500 °C caused reduction to occur at much higher temperatures and Pd–Re alloy particles were formed [18].

Quantitative H₂ uptake measurements on the bimetallic catalysts indicate that >90% of the Re was reduced to the zero-valent state after TPR to 400 °C (Table 2). Residual Re⁷⁺ species interacting strongly with the support and intermediate Re oxidation states (e.g., Re⁴⁺) cannot be completely excluded.

TPHD measurements were performed on the 3 wt.% Pd/Al₂O₃ catalysts after TPR to 400 °C. The TPHD spectrum of Pd3-N comprises a sharp H₂ evolution peak at ~55 °C with a shoulder at ~50 °C. The H/Pd ratio (Table 2) is approximately half that observed in bulk Pd (H/Pd = 0.65) under similar conditions [17,18]. In contrast, the TPHD spectrum of Pd3-TA comprises a broad asymmetric H₂ evolution peak centered around ~30 °C and a small sharp peak at ~55 °C. The H/Pd ratio is less than half that for Pd3-N (Table 2) consistent with highly dispersed supported Pd [35]. We assign the broad low-temperature peak to the decomposition of supported PdH_x nanoparticles and the small peak at 55 °C to larger supported Pd crystallites. A lower decomposition temperature indicates lower stability of the PdH_x phase in supported nanoparticles.

Re addition via any of the methods employed herein alters the H/Pd ratio and stability of the bulk PdH_x phase. Alloying Pd with other transition metals (e.g., Au) is known to alter its electronic structure and destabilize the bulk hydride phase. The highest concentration of Re in PdRe solid solutions is ~10% [36]; however, bulk thermodynamics may not apply to small particles [37]. Ziemecki et al. employed H₂ uptake during cooling in the TPR apparatus to assess hydride suppression and infer alloy formation in PdAu and PdRe catalysts [17]. Malinowski et al. [13] used a second TPR (equivalent to our TPHD) to characterize PdRe/Al₂O₃ catalysts and reported a reduction in the H/Pd ratio and destabilization of the hydride phase with increasing Re content. TPHD measurements on bimetallic catalysts prepared by using Pd(NO₃)₂ are shown in Figure 3a. For both catalysts, there is a significant reduction in the Pd/H ratio (Table 2) and a low-temperature shift in decomposition temperature relative to Pd3-N. These observations are consistent with a strong PdRe bulk interaction, i.e., alloy formation in Pd-rich particles. TPHD spectra of more highly dispersed bimetallic catalysts are shown in Figure 3b. PdH_x formation is completely suppressed in the 2:1 Re:Pd (bulk atomic ratio) catalyst prepared from the DCS [38]. The TPHD spectrum of Pd3Re5-SI suggests a strong PdRe interaction; hydride formation is strongly suppressed, and decomposition occurs at much lower temperatures than typical for PdH_x nanoparticles. Ziemecki et al. reported equivalent observations for a similarly prepared PdRe/Al₂O₃ catalyst lending support to the Re₂O₇ surface mobility hypothesis [18]. In contrast, the TPHD spectra of Re5Pd3-SI (350) and Re5Pd3-SI (400) contain a single sharp decomposition peak at 40–50 °C consistent with PdH_x particles, and the H/Pd ratios (Table 2) are equivalent to that of Pd3-TA. These results do not suggest bulk alloy formation and are consistent with low-temperature Re reduction via hydrogen spillover from vicinal Pd nanoparticles.

CO and H₂ chemisorption data are provided in Table 3. The data confirm that Pd3-TA is more highly dispersed than Pd3-N, as expected from Raman spectroscopy and TPR. The CO/Pd ratio for Pd1-N is approximately three times higher than for Pd3-N indicating that lowering the Pd loading increases dispersion, as expected. At 35 °C, the H/CO ratios are approximately unity for Pd3-N and Pd1-N. H₂ chemisorption uptake declined by ~30% for these catalysts at 100 °C. The low CO/Re ratio for Re5-N is consistent with previous volumetric chemisorption data on Re/Al₂O₃ [21]. The H/CO ratio for Re5-N at 35 °C is only ~15%, but H₂ uptake increases at 100 °C consistent with activated dissociative chemisorption [39].

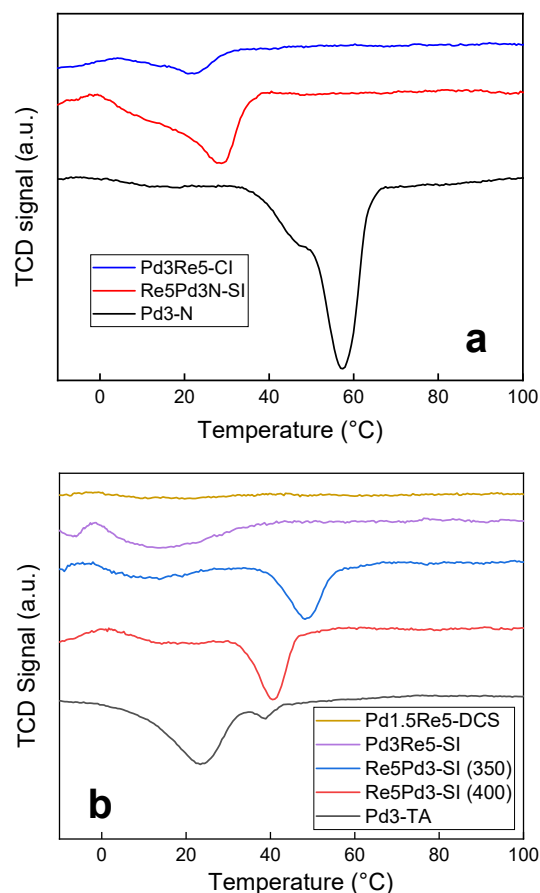


Figure 3. TPHD spectra for catalysts prepared from $\text{Pd}(\text{NO}_3)_2$ (a) and $\text{Pd}(\text{NH}_3)_4(\text{NO}_3)_2$ (b) after TPR to 400 °C and cooling in 5% H_2/Ar .

Table 3. CO and H_2 chemisorption results.

Catalyst	CO Chemisorption		H ₂ Chemisorption					
	35 °C		35 °C		100 °C			
	CO Uptake ^a	CO/Metal	H ₂ uptake ^a	H/Metal	H/CO	H ₂ Uptake	H/Metal	H/CO
Pd1-N	28.5	0.333	12.7	0.297	0.89	8.8	0.204	0.62
Pd3-N	32.4	0.130	16.7	0.133	1.03	12.4	0.100	0.76
Pd3-TA	103	0.469	45.0	0.370	0.88	34.0	0.280	0.66
Pd3Re5-CI	59.0	0.127	26.7	0.115	0.90	27.3	0.117	0.92
Pd3Re5-SI	80.5	0.157	17.9	0.070	0.44	21.6	0.084	0.54
Re5Pd3N-SI	50.5	0.099	n/a	-	-	n/a	-	-
Re5Pd3-SI (350)	96.2	0.206	20.9	0.089	0.43	26.7	0.114	0.56
Re5Pd3-SI (400)	92.6	0.210	20.3	0.092	0.44	21.1	0.096	0.46
Pd1.5Re5-DCS	44.6	0.116	7.6	0.040	0.34	11.0	0.057	0.49
Re5-N	33.8	0.139	2.3	0.019	0.14	14.5	0.119	0.86

^a units: $\mu\text{mol/g}$.

The CO uptakes of Pd3Re5-CI and Re5Pd3N-SI are greater than Pd3-N indicating either a significant Re-CO contribution and/or smaller Pd particle size. In contrast, Pd3Re5-SI has lower CO uptake than Pd3-TA notwithstanding Re addition. The CO uptakes for Re5Pd3-SI (400) and Re5Pd3-SI (350) are only ~10% lower than Pd3-TA. H₂ chemisorption is strongly suppressed (relative to CO chemisorption) on the Pd3Re5-SI, Re5Pd3-SI (400), Re5Pd3-SI (350) and Pd1.5Re5-DCS catalysts suggesting Re coverage of the supported Pd particles. Re addition to Pd/ Al_2O_3 catalysts is known to suppress H₂ chemisorption [13,14], and we have provided evidence that Re blocks surface sites on Pd particles [21]. The H/CO ratios observed for the bimetallic catalysts in this work, except Pd3Re5-CI, are ~0.4 at 35 °C

and ~ 0.5 at 100°C consistent with suppression of H_2 chemisorption. The chemisorptive properties of Pd3Re5-CI are more consistent with supported Pd than a bimetallic catalyst.

In general, the Kubelka–Munk (K–M) intensities of the CO DRIFT spectra are consistent with the CO chemisorption uptakes ($\mu\text{mol}/\text{g}_{\text{cat}}$) of the catalysts. Catalysts prepared using Pd tetraammine (including the DCS) (Figure 4a) have more intense $\nu(\text{CO})$ peaks than catalysts prepared from $\text{Pd}(\text{NO}_3)_2$ (Figure 4b). For Pd3-TA, the linear (atop) CO peak ($\sim 2080\text{ cm}^{-1}$) is more intense than the broad bridging CO band ($\sim 1930\text{ cm}^{-1}$) consistent with highly dispersed supported Pd [40–42]. The 1930-cm^{-1} band and its low-frequency tail (extending to 1700 cm^{-1}) are associated with doubly and triply bridging CO species on Pd nanoparticles. The CO DRIFT spectrum of Re5Pd3-SI (400) is closely similar albeit of lower intensity. A significant enhancement of the linear-to-bridging (L/B) ratio and a blueshift of the bridging CO band to $\sim 1950\text{ cm}^{-1}$ are observed for Pd3Re5-SI. We infer that these trends indicate surface modification by Re adatoms leaving fewer adjacent Pd atoms to accommodate bridging CO species. The blueshift probably arises from decreased dipolar coupling between bridging CO moieties. The CO DRIFT spectrum of Pd1.5Re5-DCS is qualitatively similar, but the peak intensities are much lower consistent with its lower Pd loading. Only a small shoulder at $\sim 2040\text{ cm}^{-1}$ assigned to CO linearly adsorbed on metallic Re particles is observed for these catalysts [38,43]. There are several potential explanations: $[\text{ReO}_4]^-$ (or Re_2O_7) species spread over the $\gamma\text{-Al}_2\text{O}_3$ surface during calcination, and reduction of isolated $[\text{ReO}_4]^-$ species is incomplete at 400°C [27,44]. Alternatively, re-oxidation of Re metal centers (single atoms, clusters) can occur during the He purge at 400°C after in situ reduction [38,44].

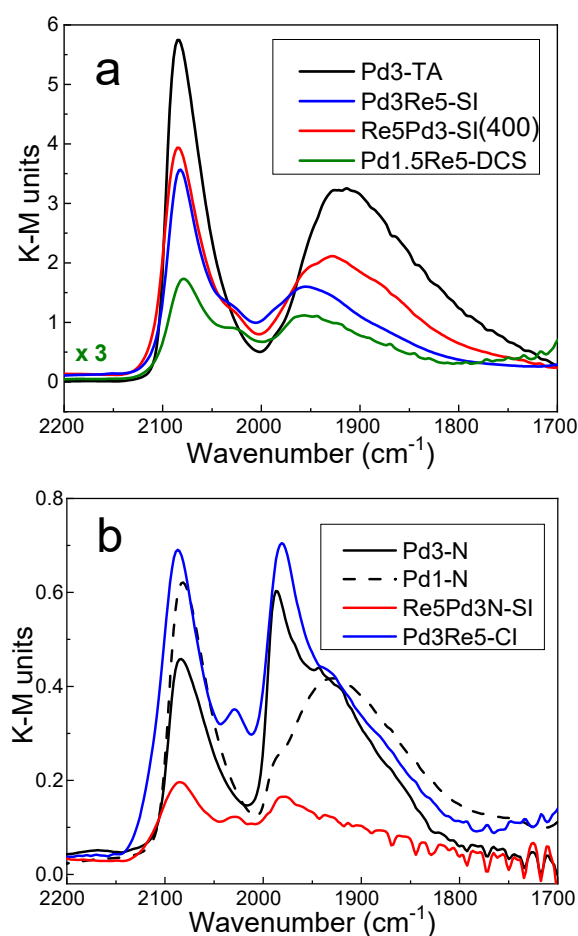


Figure 4. DRIFT spectra of adsorbed CO at 20°C : (a) catalysts prepared from $\text{Pd}(\text{NH}_3)_4(\text{NO}_3)_2$ and DCS and (b) catalysts prepared from $\text{Pd}(\text{NO}_3)_2$. Catalysts were pretreated in situ in flowing H_2 at 400°C .

The CO DRIFT spectrum of Pd3-N comprises linear and bridging bands (Figure 4b), and the latter are dominant. The prominent 1990-cm^{-1} peak corresponds to bridging CO on low-index surface planes [e.g., (100) and (111)] of supported Pd crystallites [41,42]. The strong shoulder at 1930 cm^{-1} is equivalent to that observed for supported Pd nanoparticles (Figure 4a). For Pd1-N, conversely, there is only a medium shoulder at 1990 cm^{-1} , and the 1930 cm^{-1} bridging band is more prominent. The L/B ratio is also higher consistent with its higher dispersion. The CO DRIFT spectrum of Pd3Re5-CI contains strong peaks at 2080 and 1990 cm^{-1} assigned to linear and doubly bridging CO, and the L/B ratio is higher when compared to Pd3-N. A medium-intensity peak at $\sim 2040\text{ cm}^{-1}$ is assigned to linear CO on Re [38,43]. We infer that coverage of Pd particles by Re (or alloying) results in fewer adjacent Pd atoms exposed, thereby increasing the L/B ratio. The CO DRIFT spectrum of Re5Pd3N-SI is qualitatively similar with linear and bridging Pd-CO bands and a small linear Re-CO peak at $\sim 2040\text{ cm}^{-1}$.

Low-magnification HAADF-STEM images of Pd3Re5-SI and Re5Pd3-CI catalyst particles (Figure 5) provide visual evidence of the much higher metal dispersion and more uniform distribution in the former. Small bright scattering centers (metal particles) are observed uniformly covering the $\gamma\text{-Al}_2\text{O}_3$ support in Figure 5a. In contrast, larger metal particles are seen near the particle edges in Figure 5b. Figure 6a displays a higher magnification HAADF image of Pd3Re5-CI showing two large (20–30 nm) and many small metal particles (<5 nm) distributed across the support. The composite EDX image (Figure 6b) clearly identifies the small particles as Re, whereas the two large particles (crystallites) contain primarily Pd. The intense yellow pixels associated with the Pd particles result from the superposition of red (Pd) and green (Re) pixels. Although this image provides no depth resolution, it is clear that there are patches of Re (or ReO_x) on the larger Pd particles. Based on the TPHD results for Pd3Re5-CI (strong suppression of bulk hydride formation), it is probable that the larger bimetallic particles are alloyed. Much smaller (<5 nm) segregated Re and Pd particles are found in other regions of the $\gamma\text{-Al}_2\text{O}_3$ support, as illustrated in Figure 6c,d.

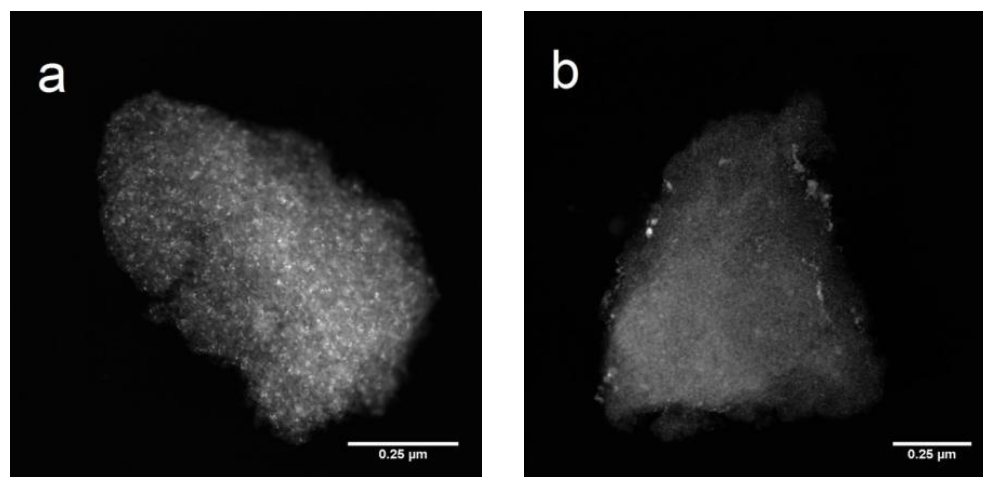


Figure 5. Low-magnification HAADF-STEM images of individual catalyst particles: (a) Re5Pd3-SI (400) and (b) Pd3Re5-CI.

The HAADF image and EDX maps of another Re5Pd3-SI (400) particle (Figure 7) reveal remarkably uniform distributions of Pd and Re nanoparticles on the $\gamma\text{-Al}_2\text{O}_3$ support. The Pd particles appear discrete, whereas the Re coverage appears nearly continuous. The supported nanoparticles are <5 nm in size, as seen in the high-magnification HAADF image in Figure 8a. The EDX map (Figure 8b) suggests that Pd and Re are segregated within the supported bimetallic nanoparticles—consistent with the TPHD results indicating no suppression of hydride formation.

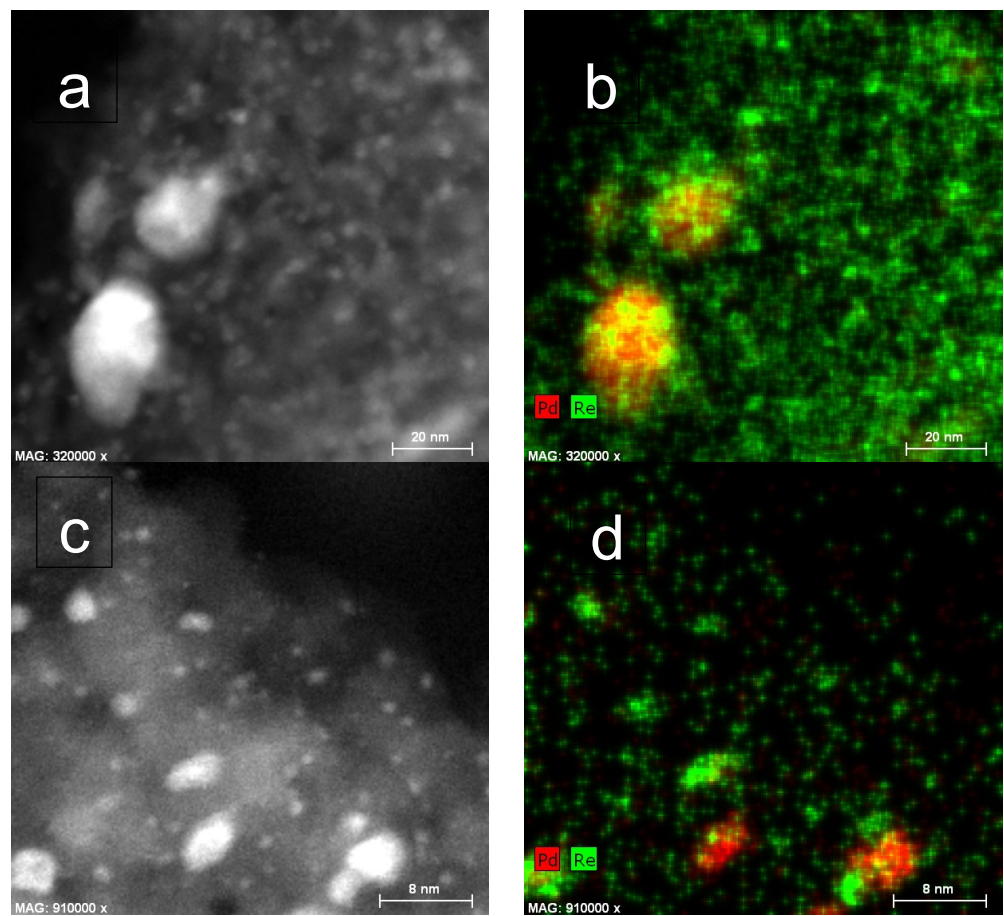


Figure 6. STEM images of Pd₃Re₅-CI: HAADF images (a,c) and composite EDX images (b,d). Color code: red—Pd, green—Re, yellow—superposition.

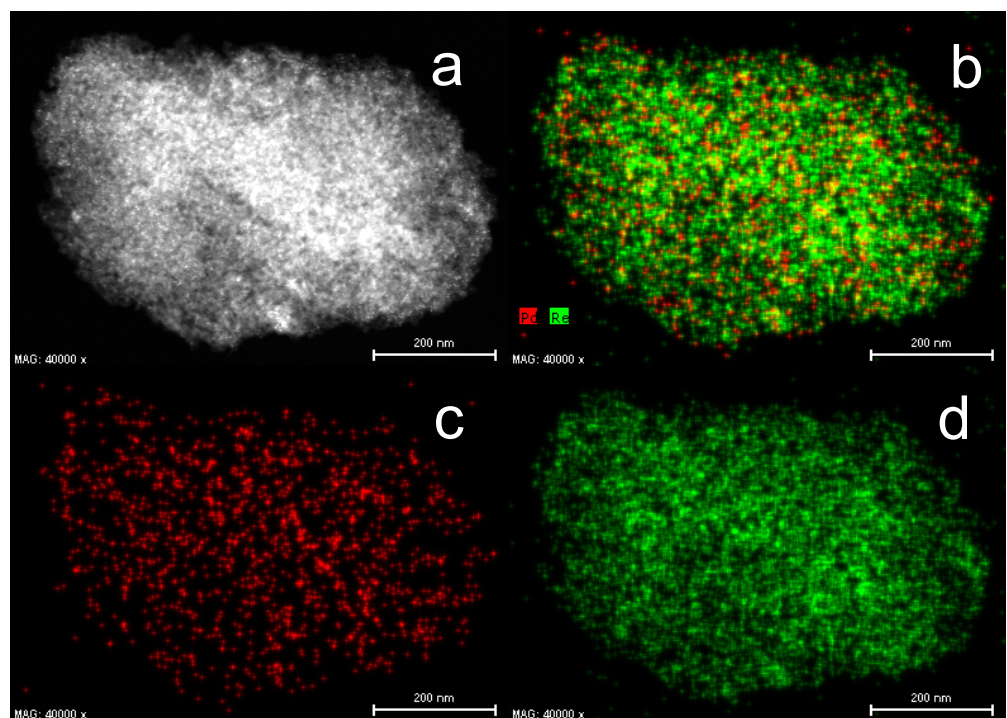


Figure 7. STEM of Re₅Pd₃-SI (400) catalyst: HAADF image (a), composite EDX map (b), Pd EDX map (c), and Re EDX map (d). Color code: Pd (red) and Re (green).

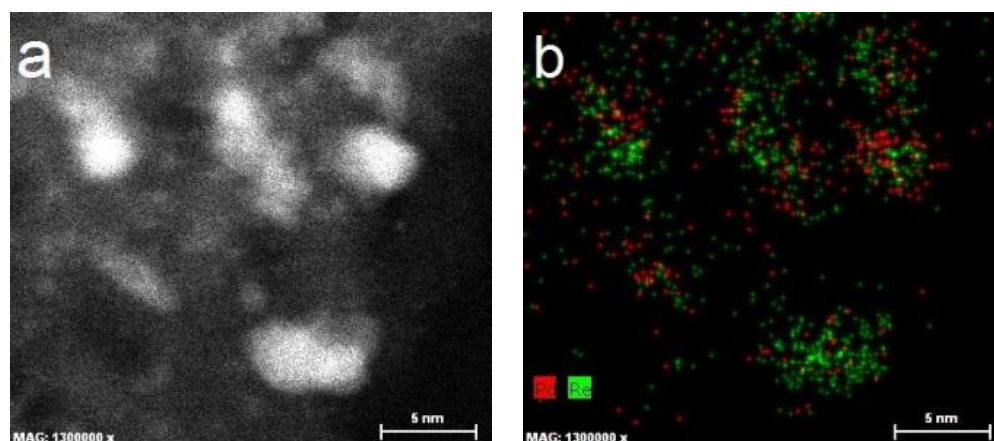
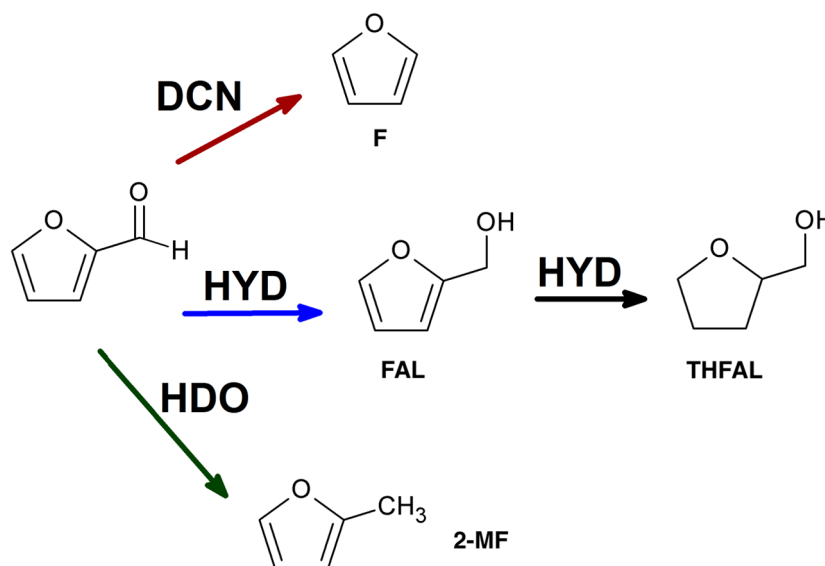


Figure 8. High-magnification STEM of Re₅Pd₃-SI (400) catalyst: HAADF image (a) and corresponding EDX map (b) showing Pd (red) and Re (green).

2.2. Furfural Hydrogenation Catalysis

Three reaction pathways were inferred for furfural conversion over Pd/Al₂O₃ and PdRe/Al₂O₃ catalysts under the investigated conditions (Scheme 1). Ring-opening products (e.g., butanols and pentanols) were not observed. Furan (F), furfuryl alcohol (FAL), and tetrahydrofurfuryl alcohol (THFAL) were identified as primary products over Pd/Al₂O₃ via the Delplot method [21]. Furfural decarbonylation (DCN) produces F and CO. Selective hydrogenation (HYD) to FAL is the desired pathway. A third pathway is direct hydrodeoxygenation (HDO) to 2-methylfuran (2-MF). 2-MF was a primary product only over Pd₃-N and the Re-containing catalysts. Selectivity to other ring-saturation products: tetrahydrofuran (THF) and 2-methyl THF (2-MTHF) was generally low indicating secondary products. Re₅-N was essentially inactive relative to the Pd/Al₂O₃ and PdRe/Al₂O₃ catalysts.



Scheme 1. Furfural catalytic reaction pathways: decarbonylation (DCN), hydrogenation (HYD), and hydrodeoxygenation (HDO). Only primary products are shown.

Product formation rates for the Pd/Al₂O₃ and PdRe/Al₂O₃ catalysts are shown in Figure 9; the total bar height represents the furfural consumption rate for each catalyst. The Pd/Al₂O₃ catalysts (irrespective of precursor) and Pd₃Re₅-CI (Figure 9a) were far less active than the bimetallic catalysts prepared from the DCS and by SI (Figure 9b). The higher activities of the latter are likely because of their higher metal dispersions. The similar activities of the Pd₃-N and Pd₃-TA catalysts are surprising given the much higher

dispersion of the latter. Furan was the main product over the Pd1-N and Pd3-N catalysts, and the order of relative abundance was F + THF > FAL + THFAL >> 2-MF. Over Pd3-TA, the order was FAL + THFAL > F + THF > 2-MF showing a modest preference for aldehyde group HYD over DCN. Significantly, F production was suppressed markedly over all the bimetallic catalysts regardless of activity. For example, the Pd3-N and Pd3Re5-CI catalysts both have similar low activities, but the latter has much greater FAL selectivity and far lower F selectivity. All the bimetallic catalysts strongly favored HYD over DCN with the order of relative product abundance: FAL + THFAL >> F + THF ~ 2-MF. This product distribution is more consistent with Re (rather than Pd) catalysis [21]. The DCS-derived catalyst was most selective to FAL (78.3%) and exhibited 93% selectivity to FAL + THFAL. The Pd3Re5-SI and Re5Pd3-SI (350) catalysts had similar activities and FAL selectivities indicating that the impregnation sequence is relatively unimportant. The Re5Pd3-SI (400) catalyst (that was calcined at 400 °C for 3 h after each impregnation step) was more active but less selective to FAL; however, its FAL + THFAL selectivity (81%) was comparable to the other SI catalysts. The Pd3Re5-SI catalyst prepared from the Pd(NH₃)₄(NO₃)₂ precursor was more active and more selective than a SI catalyst derived from Pd(NO₃)₂ reported previously [21]. The Re-first SI and the DCS-derived catalysts are modestly (~20%) more active with ~10% greater FAL selectivity than those reported previously [21]. We speculate that this could be a promoter effect of the Group I or IIA metal impurities in γ -Al₂O₃ (A) [11].

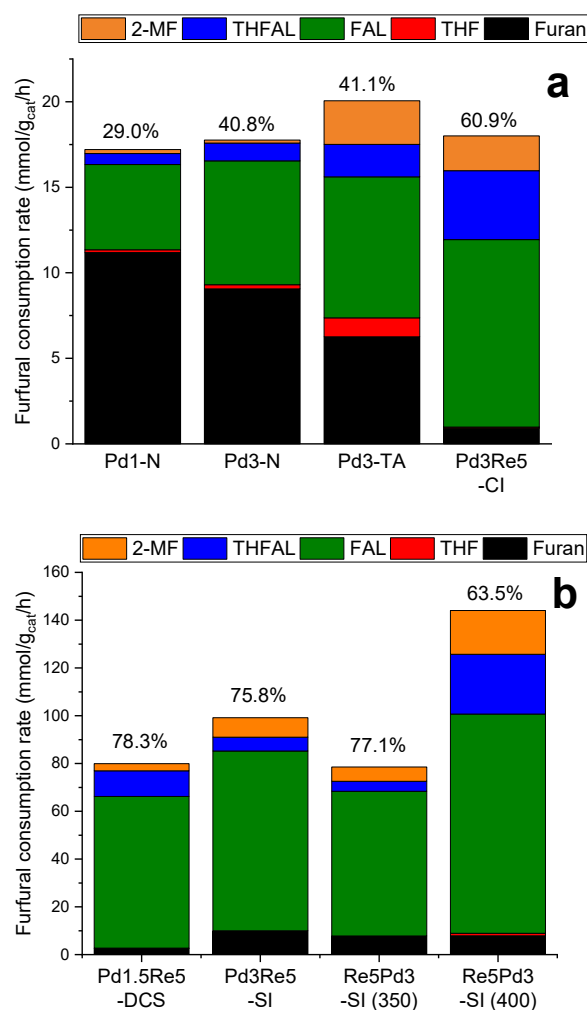


Figure 9. Furfural consumption rates and product formation rates at 150 °C and 1 atm: Pd/Al₂O₃ catalysts and Pd3Re5-CI (a) and other PdRe/Al₂O₃ catalysts (b). FAL selectivities are indicated above the bars.

Turnover frequencies (TOFs) for furfural consumption at 150 °C are given in Table 4. The TOF(CO) values (based on CO adsorption isotherms measured at 35 °C) are in excellent agreement for the Pd1-N and Pd3-N catalysts and in good agreement with those previously reported for Pd/Al₂O₃ catalysts [21]. Moreover, their TOF(H) values (per H atom based on H₂ dissociative chemisorption at 35 °C) are also in excellent agreement (with each other and the TOF(CO) values). The origin of the lower intrinsic activity of Pd3-TA is unknown, but the TOFs are within a factor of 2 of those reported previously for a similar catalyst prepared on γ -Al₂O₃ (B) [21]. The TOF(CO) values of all the PdRe/Al₂O₃ catalysts except Pd3Re5-CI are 2–5 times higher than those of the Pd/Al₂O₃ catalysts. In contrast to the Pd/Al₂O₃ catalysts, the TOF(H) values (per H atom based on H₂ dissociative chemisorption at 100 °C) are approximately two times higher than the TOF(CO) values for these PdRe/Al₂O₃ (except Pd3Re5-CI) because of H₂ chemisorption suppression (Table 3). The TOFs for Pd3Re5-CI are equivalent, lower and in better agreement with those of the Pd/Al₂O₃ catalysts. We infer that Pd3Re5-CI has lower intrinsic activity (and somewhat lower FAL selectivity) because it contains a mixture of supported bimetallic alloy and homometallic nanoparticles. The TOFs for Pd3Re5-SI agree very closely with those reported previously for an analogous catalyst prepared using a 3 wt.% Pd/Al₂O₃ catalyst derived from Pd(NO₃)₂ [21]. Finding equivalent TOFs despite large differences in Pd dispersion validates using CO and H₂ chemisorption for counting active sites. Both SI methods produce highly active and selective catalysts. The highly dispersed PdRe/Al₂O₃ prepared by impregnation with the DCS exhibits the highest intrinsic activity and FAL selectivity. We infer that intimate contact between supported Pd and Re nanoparticles results in suppression of Pd-catalyzed decarbonylation and creates Pd–Re sites with high intrinsic activity. Our results are consistent with the proposal that Pd facilitates the reaction via H₂ dissociation and spillover of H species onto vicinal Re sites [22].

Table 4. TOFs for furfural consumption at 150 °C measured under differential conversion (<10%) conditions.

Catalyst	TOF (min ⁻¹) ^a	
	CO	H
Pd1-N	10.1	11.3 ^b
Pd3-N	9.1	8.9 ^b
Pd3-TA	3.2	3.7 ^b
Pd3Re5-CI	5.1	5.5
Pd3Re5-SI	20.5	38.3
Re5Pd3-SI (350)	13.6	24.5
Re5Pd3-SI (400)	26.0	57.0
Pd1.5Re5-DCS	29.9	60.6

^a Basis: CO chemisorption at 35 °C and H₂ dissociative chemisorption at 100 °C (unless otherwise noted). ^b Basis: H₂ dissociative chemisorption at 35 °C.

3. Materials and Methods

3.1. Catalyst Preparation

The γ -Al₂O₃ support (BET surface area and total pore volume of 217 m²/g and 0.47 cm³/g, respectively) was purchased from Strem Chemicals (Newburyport, MA, USA). Elemental analysis by inductively coupled plasma-optical emission spectrometry (ICP-OES) revealed the following alkali metal and alkaline earth metal impurities: 213 ppm Na, 24.0 ppm Mg, 8.32 ppm K, and 132 ppm Ca. The mono- and bimetallic catalysts were prepared by IW impregnation, except for the Pd1.5Re5-DCS catalyst which was prepared by wet impregnation with [Pd(NH₃)₄(ReO₄)₂], as described elsewhere [38]. For the bimetallic catalysts, three different IW methods and precursors were employed: (i) co-impregnation using Pd(NO₃)₂ and HReO₄, (ii) Re-first sequential impregnation using NH₄ReO₄ and [Pd(NH₃)₄(NO₃)₂], and (iii) HReO₄ addition to a reduced and passivated Pd/Al₂O₃ catalyst. These methods are described in more detail elsewhere [21]. For comparison, a catalyst (Re5Pd3N-SI) was also prepared by Re-first sequential impregnation using HReO₄ and

$\text{Pd}(\text{NO}_3)_2$. The Pd tetraammine nitrate, $\text{Pd}(\text{NO}_3)_2$, and $\text{Pd}(\text{NO}_3)_2 + \text{HReO}_4$ impregnation solutions were pH 10, pH 7, and pH 1, respectively. Typically, after each impregnation step the catalysts were dried at 110 °C overnight, crushed with mortar and pestle, and calcined at 400 °C for 3 h in flowing zero-grade air. Re5Pd3-SI (350) was calcined at 350 °C for 1 h, and the Pd1.5Re5-DCS and Pd3Re5-SI catalysts were not calcined. All catalysts were stored in a desiccator prior to use. ICP-OES analyses for Pd and Re were performed by Eastman Chemical Company (Kingsport, TN, USA).

3.2. TPR and TPHD

TPR and TPHD experiments were performed using a Micromeritics 2920 Autochem II (Norcross, GA, USA) equipped with a thermal conductivity detector (TCD) for monitoring H_2 uptake/evolution. Catalyst samples (100 mg) were cooled to -50 °C in ultra-high purity He (Airgas, RTP, NC, USA), and the feed gas was switched to 5% H_2/Ar (certified mixture, Machine and Welding Supply). Both gases were purified using inline $\text{H}_2\text{O}/\text{O}_2$ traps. After waiting for the TCD baseline to stabilize, the sample was heated at 10 °C/min to 400 °C and held for 1 h. Select Re-containing catalysts were heated to 800 °C to ensure complete reduction was achieved. After TPR to 400 °C, Pd-containing catalysts were cooled to -50 °C in 5% H_2/Ar and purged with Ar. Subsequently, TPHD spectra were measured using the TCD and a temperature ramp of 10 °C/min to 400 °C in flowing Ar.

3.3. CO and H_2 Chemisorption

Volumetric H_2 and CO chemisorption measurements were performed using a Micromeritics ASAP 2020c instrument (Norcross, GA, USA). Each catalyst was reduced in situ in flowing research-grade H_2 (50 sccm) at 400 °C for 1 h, evacuated at 400 °C for 2 h using a turbomolecular pump, and then cooled to 100 °C for H_2 analysis. The H_2 analysis was repeated at 70 °C and 35 °C, and the sample was evacuated at 300 °C for 1 h between each analysis. Subsequently, CO adsorption isotherms were measured at 35 °C. Adsorption isotherms were measured before and after evacuation at the analysis temperature; the difference was used to determine strongly adsorbed species.

3.4. CO DRIFTS

DRIFT spectra of adsorbed CO were measured on a Bruker Vertex 70 FTIR (Billerica, MA, USA) with a liquid N_2 -cooled MCT detector using a Harrick Praying Mantis cell (Pleasantville, NY, USA). Prior to measurement, samples were reduced in situ the DRIFTS cell at 400 °C for 1 h in 40 sccm H_2 (research grade, National Welders), then purged in He at 40 sccm (UHP, Airgas, RTP, NC, USA) for 1 h before cooling to 20 °C. Pulses of 5% CO/He (certified, Airgas, RTP, NC, USA) were administered five at a time at 20 °C until no further changes in spectra were observed. Scans of the reduced catalyst (128 scans at 4-cm^{-1} resolution) at 20 °C in He were subtracted from scans following pulses of CO in order to subtract out signal from H_2O .

3.5. Raman Spectroscopy

Raman spectra of the powder samples were recorded on a Horiba Jobin-Yvon LabRAM HR VIS (Kyoto, Japan) high-resolution confocal Raman microscope (using a He–Ne laser (632 nm) excitation source and 100× objective. The laser power was 20 mW, and the confocal hole size was 800 μm . The instrument was calibrated using a Si wafer at 520.7 cm^{-1} . The exposure time was 15 s at a resolution of 0.1 cm^{-1} . Catalyst samples were removed from the storage desiccator and handled and scanned in ambient air. No spectral degradation was observed during data collection. Raman bands due to the $\gamma\text{-Al}_2\text{O}_3$ support were removed by spectral subtraction.

3.6. HAADF-STEM-EDX

High-resolution STEM imaging was performed on an aberration-corrected FEI Titan 80–300 electron microscope (Hillsboro, OR, USA). The microscope is equipped with a

high-angle annular dark field (HAADF) detector and SuperX EDS system comprising four Bruker silicon drift detectors. Samples were reduced ex situ at 400 °C, and handled under N₂, except for brief exposure during insertion into the microscope. The powder was supported on carbon-coated copper grids (Ted Pella, Redding, CA, USA).

3.7. Furfural Hydrogenation

Furfural hydrogenation activity was tested in a continuous flow packed-bed reactor system at 150 °C and atmospheric pressure. The catalyst bed comprised 50–250 mg catalyst powder and 1.25 g quartz chips and was supported by quartz wool in a 0.5" stainless steel tube. Catalyst bed temperature was measured by a Type-K thermocouple (Omega, Norwalk, CT, USA) in contact with the catalyst inside the tube. Furfural was fed by a syringe pump, vaporized in a stream of 100% H₂, and passed over the catalyst bed. The effluent was monitored by two on-line gas chromatographs (GCs): GC-TCD (SRI 8610C) with a ShinCarbon ST100 (2 m × 1.0 mm ID) column (Restek, Bellefonte, PA, USA) measured CO, CH₄, and CO₂; a GC-FID (Shimadzu 2010, Columbia, MD, USA) with an EconoCap-1 column (30 m × 0.53 mm ID, Grace Alltech, Aiken, SC, USA) measured all other products.

4. Conclusions

PdRe/Al₂O₃ catalysts for selective hydrogenation of furfural combine synergistically: (1) inhibition of Pd-catalyzed decarbonylation by Re and (2) promotion of Re hydrogenation activity by Pd. Raman spectra of the calcined catalysts evidence that (1) the Pd(NO₃)₂ precursor results in large supported PdO crystallites and (2) either Re precursor results in supported [ReO₄][−] (perrhenate) species. The latter exist in hydrated and dehydrated forms. The Raman spectra subsequently inform TPR peak assignments. TPR profiles beginning at low temperatures capture the reduction of supported PdO crystallites (which occurs at <0 °C for Pd₃-N). H₂ absorbed to form PdH_x evolves at higher temperatures resulting in no net consumption. The observed CO DRIFTS bands can be assigned to either Pd_n-CO (*n* = 1, 2, 3) or Re-CO moieties. Bridging carbonyls on Pd sites are strongly suppressed in the most active bimetallic catalysts. Optimum catalysts comprise supported bimetallic nanoparticles, and bulk alloy formation is not required, as evidenced by TPHD. A low-dispersion PdRe/Al₂O₃ catalyst containing supported Pd-Re alloy crystallites (as indicated by TPHD and HAADF-STEM) exhibited a furfural TOF similar to Pd/Al₂O₃ albeit with higher FAL selectivity.

Author Contributions: Conceptualization, H.H.L. and S.T.T.; Formal analysis, S.T.T.; Funding acquisition, H.H.L.; Investigation, S.T.T.; Methodology, S.T.T. and H.H.L.; Supervision, H.H.L. All authors have read and agreed to the published version of the manuscript.

Funding: This work was funded by the Eastman Chemical Company through the Center of Excellence at North Carolina State University. ICP-OES analysis was performed by Eastman Chemical Company in Kingsport, TN. The authors acknowledge the use of the Analytical Instrumentation Facility at NCSU, which is supported by the State of North Carolina and the National Science Foundation.

Data Availability Statement: All pertinent data are provided in the manuscript.

Acknowledgments: Xiahan Sang for assistance with STEM-EDX.

Conflicts of Interest: The authors declare no conflict of interest.

References

1. Chen, K.Y.; Koso, S.; Kubota, T.; Nakagawa, Y.; Tomishige, K. Chemoselective Hydrogenolysis of Tetrahydropyran-2-methanol to 1,6-Hexanediol over Rhenium-Modified Carbon-Supported Rhodium Catalysts. *Chemcatchem* **2010**, *2*, 547–555. [[CrossRef](#)]
2. Koso, S.; Nakagawa, Y.; Tomishige, K. Mechanism of the hydrogenolysis of ethers over silica-supported rhodium catalyst modified with rhenium oxide. *J. Catal.* **2011**, *280*, 221–229. [[CrossRef](#)]
3. Chia, M.; Pagan-Torres, Y.J.; Hibbitts, D.; Tan, Q.H.; Pham, H.N.; Datye, A.K.; Neurock, M.; Davis, R.J.; Dumesic, J.A. Selective Hydrogenolysis of Polyols and Cyclic Ethers over Bifunctional Surface Sites on Rhodium–Rhenium Catalysts. *J. Am. Chem. Soc.* **2011**, *133*, 12675–12689. [[CrossRef](#)]

4. Koso, S.; Furikado, I.; Shima, A.; Miyazawa, T.; Kunimori, K.; Tomishige, K. Chemoselective hydrogenolysis of tetrahydrofurfuryl alcohol to 1,5-pentanediol. *Chem. Comm.* **2009**, 2035–2037. [[CrossRef](#)] [[PubMed](#)]
5. Ma, L.; He, D.H.; Li, Z.P. Hydrogenolysis of bioglycerol to 1,2-propanediol over Ru/CeO₂ catalysts: Influence of CeO₂ characteristics on catalytic performance. *Catal. Comm.* **2008**, *9*, 2489–2495. [[CrossRef](#)]
6. Ma, L.; He, D.H. Hydrogenolysis of Glycerol to Propanediols Over Highly Active Ru–Re Bimetallic Catalysts. *Top. Catal.* **2009**, *52*, 834–844. [[CrossRef](#)]
7. Takeda, Y.; Nakagawa, Y.; Tomishige, K. Selective hydrogenation of higher saturated carboxylic acids to alcohols using a ReOx–Pd/SiO₂ catalyst. *Catal. Sci. Technol.* **2012**, *2*, 2221–2223. [[CrossRef](#)]
8. Shima, A.; Koso, S.; Ueda, N.; Shinmi, Y.; Furikado, I.; Tomishige, K. Catalytic glycerol hydrogenolysis to 1,3-propanediol in a gas–solid fluidized bed. *Chem. Lett.* **2009**, *38*, 540–541. [[CrossRef](#)]
9. Koso, S.; Watanabe, H.; Okumura, K.; Nakagawa, Y.; Tomishige, K. Preferential CO Oxidation in a H₂-Rich Stream on Pt–ReOx/SiO₂: Catalyst Structure and Reaction Mechanism. *J. Phys. Chem. C* **2012**, *116*, 3079–3090. [[CrossRef](#)]
10. Ly, B.K.; Minh, D.P.; Pineda, C.; Besson, M.; Tapin, B.; Epron, F.; Especel, C. Effect of Addition Mode of Re in Bimetallic Pd–Re/TiO₂ Catalysts Upon the Selective Aqueous-Phase Hydrogenation of Succinic Acid to 1,4-Butanediol. *Top. Catal.* **2012**, *55*, 466–473. [[CrossRef](#)]
11. Mabry, M.A.; Prichard, W.W.; Ziemecki, S.B. Process for Making Tetrahydrofuran and 1,4-Butanediol Using Pd/Re Hydrogenation Catalyst. U.S. Patent 4,550,185, 29 October 1985.
12. Kitson, M.; Williams, P.S. Platinum Group Metal Alloy Catalysts for Hydrogenation of Carboxylic Acids and Their Anhydrides to Alcohols and/or Esters. U.S. Patent 5,149,680, 22 September 1992.
13. Malinowski, A.; Juszczak, W.; Bonarowska, M.; Pielaszek, J.; Karpinski, Z. Pd–Re/Al₂O₃: Characterization and catalytic activity in hydrodechlorination of CCl₂F₂. *J. Catal.* **1998**, *177*, 153–163. [[CrossRef](#)]
14. Bonarowska, M.; Malinowski, A.; Karpinski, Z. Hydrogenolysis of C–C and C–Cl bonds by Pd–Re/Al₂O₃ catalysts. *Appl. Catal. A* **1999**, *188*, 145–154. [[CrossRef](#)]
15. Juszczak, W.; Karpinski, Z. Hydrocarbon reactions on Pd–Re/Al₂O₃ catalysts. *Appl. Catal. A* **2001**, *206*, 67–78. [[CrossRef](#)]
16. Meitzner, G.; Via, G.H.; Lytle, F.W.; Sinfelt, J.H. Structure of bimetallic clusters. Extended x-ray absorption fine structure (EXAFS) of Pt–Re and Pd–Re clusters. *J. Chem. Phys.* **1987**, *87*, 6354–6363. [[CrossRef](#)]
17. Ziemecki, S.B.; Michel, J.B.; Jones, G.A. Hydride formation as a measure of alloying in bimetallic systems containing Palladium. *React. Sol.* **1986**, *2*, 187–202. [[CrossRef](#)]
18. Ziemecki, S.B.; Jones, G.A.; Michel, J.B. Effect of Phosphorus Content in Nickel Phosphide Catalysts Studied by XAFS and Other Techniques. *J. Catal.* **1986**, *99*, 207–217. [[CrossRef](#)]
19. Latusek, M.P.; Spigarelli, B.P.; Heimerl, R.M.; Holles, J.H. Correlation of H₂ heat of adsorption and ethylene hydrogenation activity for supported Re@Pd overlayer catalysts. *J. Catal.* **2009**, *263*, 306–314. [[CrossRef](#)]
20. Skoglund, M.D.; Holles, J.H. Overlayer bimetallic catalysts or particle size effects? A comparison of Re@Pd catalysts with different particle sizes. *Catal. Lett.* **2013**, *143*, 966–974. [[CrossRef](#)]
21. Thompson, S.T.; Lamb, H.H. Palladium–Rhenium Catalysts for Selective Hydrogenation of Furfural: Evidence for an Optimum Surface Composition. *ACS Catal.* **2016**, *6*, 7438–7447. [[CrossRef](#)]
22. Kammert, J.D.; Chemburkar, A.; Miyake, N.; Neurock, M.; Davis, R.J. Reaction Kinetics and Mechanism for the Catalytic Reduction of Propionic Acid over Supported ReO_x Promoted by Pd. *ACS Catal.* **2011**, *11*, 1435–1455. [[CrossRef](#)]
23. Otto, K.; Hubbard, C.P.; Weber, W.H.; Graham, G.W. Raman spectroscopy of palladium oxide on γ -alumina applicable to automotive catalysts: Nondestructive, quantitative analysis; oxidation kinetics; fluorescence quenching. *Appl. Catal. B* **1992**, *1*, 317–327. [[CrossRef](#)]
24. Baylet, A.; Marecot, P.; Duprez, D.; Castellazzi, P.; Groppi, G.; Forzatti, P. In situ Raman and in situ XRD analysis of PdO reduction and Pd⁰ oxidation supported on γ -Al₂O₃ catalyst under different atmospheres. *Phys. Chem. Chem. Phys.* **2011**, *13*, 4607–4613. [[CrossRef](#)] [[PubMed](#)]
25. Hardcastle, F.D.; Wachs, I.E.; Horsley, J.A.; Via, G.H. The structure of surface rhenium oxide on alumina from laser raman spectroscopy and x-ray absorption near-edge spectroscopy. *J. Mol. Catal.* **1988**, *46*, 15–36. [[CrossRef](#)]
26. Vuurman, M.A.; Wachs, I.E. In situ Raman spectroscopy of alumina-supported metal oxide catalysts. *J. Phys. Chem.* **1992**, *96*, 5008–5016. [[CrossRef](#)]
27. Kim, D.S.; Wachs, I.E. Surface rhenium oxide-support interaction for supported Re₂O₇ catalysts. *J. Catal.* **1993**, *141*, 419–429. [[CrossRef](#)]
28. McBride, J.R.; Hass, K.C.; Weber, W.H. Resonance-Raman and lattice-dynamics studies of single-crystal PdO. *Phys. Rev. B* **1991**, *44*, 5016–5028. [[CrossRef](#)]
29. Su, S.C.; Carstens, J.N.; Bell, A.T. A Study of the Dynamics of Pd Oxidation and PdO Reduction by H₂ and CH₄. *J. Catal.* **1998**, *176*, 125–135. [[CrossRef](#)]
30. Mamede, A.S.; Leclercq, G.; Payen, E.; Granger, P.; Grimblot, J. In situ Raman characterisation of surface modifications during NO transformation over automotive Pd-based exhaust catalysts. *J. Mol. Struct.* **2003**, *651*, 353–364. [[CrossRef](#)]
31. Arai, T.; Shima, T.; Nakano, T.; Tominaga, J. Thermally-induced optical property changes of sputtered PdOx films. *Thin Solid Films* **2007**, *515*, 4774–4777. [[CrossRef](#)]

32. Jiao, L.; Regalbuto, J.R. The synthesis of highly dispersed noble and base metals on silica via strong electrostatic adsorption: I. Amorphous silica. *J. Catal.* **2008**, *260*, 329–341. [[CrossRef](#)]
33. Okal, J.; Kepinski, L.; Krajczyk, L.; Tylus, W. Oxidation and redispersion of a low-loaded Re/ γ -Al₂O₃ catalyst. *J. Catal.* **2003**, *219*, 362–371. [[CrossRef](#)]
34. Sumner, C.; Burchett, W. Developments in the Pd Catalyzed Hydrogenation of Oxygenated Organic Compounds. *Top. Catal.* **2012**, *55*, 480–485. [[CrossRef](#)]
35. McCaulley, J.A. In-situ X-ray absorption spectroscopy studies of hydride and carbide formation in supported palladium catalysts. *J. Phys. Chem.* **1993**, *97*, 10372–10379. [[CrossRef](#)]
36. Predel, B.; Madelung, O.E. (Eds.) *Landolt-Börnstein—Group IV Physical Chemistry*; Springer: Berlin/Heidelberg, Germany, 1998.
37. Sinfelt, J.H. *Bimetallic Catalysts: Discoveries, Concepts, and Applications*; John Wiley and Sons: Hoboken, NJ, USA, 1983.
38. Thompson, S.T.; Lamb, H.H. Catalysts for selective hydrogenation of furfural derived from the double complex salt [Pd(NH₃)₄](ReO₄)₂ on γ -Al₂O₃. *J. Catal.* **2017**, *350*, 111–121. [[CrossRef](#)]
39. Chadzynski, G.W.; Kubicka, H. Chemisorption of hydrogen and oxygen on γ -alumina-supported rhenium: Part 1. Chemisorption of hydrogen. *Thermochim. Acta* **1990**, *158*, 353–367. [[CrossRef](#)]
40. Giorgi, J.B.; Schroeder, T.; Baumer, M.; Freund, H.J. Study of CO adsorption on crystalline-silica-supported palladium particles. *Surf. Sci.* **2002**, *498*, L71–L77. [[CrossRef](#)]
41. Agostini, G.; Pellegrini, R.; Leofanti, G.; Bertinetti, L.; Bertarione, S.; Groppo, E.; Zecchina, A.; Lamberti, C. Determination of the particle size, available surface area, and nature of exposed sites for silica-alumina-supported Pd nanoparticles: A multitechnical approach. *J. Phys. Chem. C* **2009**, *113*, 10485–10492. [[CrossRef](#)]
42. Lear, T.; Marshall, R.; Lopez-Sanchez, J.A.; Jackson, S.D.; Klapotke, T.M.; Baumer, M.; Rupprechter, G.; Freund, H.J.; Lennon, D. Hydrogenation catalysis on Pd nanoparticles stabilized by different crosslinked polymers. *J. Chem. Phys.* **2005**, *123*, 13.
43. Daniell, W.; Weingand, T.; Knozinger, H. Redox properties of Re₂O₇/Al₂O₃ as investigated by FTIR spectroscopy of adsorbed CO. *J. Mol. Catal.* **2003**, *204*, 519–526. [[CrossRef](#)]
44. Bare, S.R.; Kelly, S.D.; Vila, F.D.; Boldingh, E.; Karapetrova, E.; Kas, J.; Mickelson, G.E.; Modica, F.S.; Yang, N.; Rehr, J.J. Experimental (XAS, STEM, TPR, and XPS) and theoretical (DFT) characterization of supported rhenium catalysts. *J. Phys. Chem. C* **2011**, *115*, 5740–5755. [[CrossRef](#)]

Disclaimer/Publisher’s Note: The statements, opinions and data contained in all publications are solely those of the individual author(s) and contributor(s) and not of MDPI and/or the editor(s). MDPI and/or the editor(s) disclaim responsibility for any injury to people or property resulting from any ideas, methods, instructions or products referred to in the content.